Mott transition on a triangular lattice

Dimitrios Galanakis,[1] Tudor D. Stanescu,[2] and Philip Phillips[1]
[1]*Loomis Laboratory of Physics, University of Illinois at Urbana-Champaign, 1100 W. Green Street, Urbana, Illinois 61801-3080, USA*
[2]*Department of Physics, Condensed Matter Theory Center, University of Maryland, College Park, Maryland 20742-4111, USA*
(Received 2 October 2008; revised manuscript received 9 January 2009; published 19 March 2009)

We study the paramagnetic side of the phase diagram of the cobaltates, Na_xCoO_2, using an implementation of the cellular dynamical mean-field theory with a noncrossing approximation impurity solver for the one-band Hubbard model on a triangular lattice. At low doping we find that the low-energy physics is dominated by a quasi-dispersionless band generated by strong correlation physics. At half filling, we find a metal-insulator transition at a critical value of the on-site interaction $U_c=5.6\pm0.15t$ which depends weakly on the cluster size. The onset of the metallic state occurs through the growth of a coherence peak at the chemical potential. Away from half filling, in the electron-doped regime, the system is metallic with a large continuous Fermi surface as seen experimentally. Upon hole doping, a quasi-non-dispersing band emerges at the top of the lower Hubbard band and controls the low-energy physics. This band is a clear signature of non-Fermi-liquid behavior and cannot be captured by any weakly coupled approach. This quasi-dispersionless band, which persists in a certain range of dopings, has been observed experimentally. We also investigate the pseudogap phenomenon in the context of a triangular lattice and propose a general framework for discussing the pseudogap problem. This framework involves a momentum-dependent characterization of the low-energy physics and links the appearance of the pseudogap to a reconstruction of the Fermi surface without invoking any long-range order or symmetry breaking. Within this framework we predict the existence of a pseudogap for the two-dimensional Hubbard model on a triangular lattice in the weakly hole-doped regime.

DOI: 10.1103/PhysRevB.79.115116 PACS number(s): 71.20.Be, 73.43.Nq

I. INTRODUCTION

Charge carriers in the cobaltates, Na_xCoO_2, are located in two-dimensional CoO_2 layers separated by insulating layers of Na^+ ions which act as electron donors. Their structure is a triangular net of edge-sharing oxygen octahedra with the Co atoms occupying the center and the Na atoms playing the role of electron donors. The octahedral symmetry around the Co ions results in a splitting of the *d*-orbitals in two e_g and three lower-lying t_{2g} orbitals. The trigonal distortion of the CoO_2 layers further splits the t_{2g} orbitals into one a_{1g} and two lower e_g'.[1] The valence of the cobaltate ions is Co^{4-x} which means that the Fermi surface will lie in the a_{1g} orbital which will range from half to fully filled. Consequently, the cobaltates constitute a realization of strongly correlated electron physics on a triangular lattice. Across their phase diagram they exhibit a wide range of behavior[2] ranging from a paramagnetic Fermi liquid at low Na concentration *x*, a strange Fermi liquid with Curie-Weiss magnetic susceptibility for high *x* and a singular insulating state at $x=0.5$. While the paramagnetic metal exhibits some properties akin to that of a Fermi liquid, the cobaltates still remain strongly correlated systems. For example, experiment[3] and theory[4] place the hopping matrix element and the on-site repulsion at $t=0.2$ eV and $U=4$ eV, respectively.

Various angle resolved photoemission spectroscopy (ARPES) studies, which suggest a Fermi surface which consists only of a large a_{1g} hole pocket with the e_g' orbitals lying under the Fermi surface, have been performed by Qian *et al.*,[5] Yang *et al.*,[6] and Qian *et al.*[7] This is in contrast with LDA calculations[1] which suggest the existence of peripheral e_g' hole pockets. In an effort to resolve this discrepancy, several multiband dynamical mean-field theory (DMFT) studies have been performed by Ishida *et al.*[8] and Marianetti *et al.*[9] Finally a few cellular DMFT (CDMFT) calculations[10,11] address mostly the Mott transition on a triangular lattice or compare different impurity solvers.

Motivated by the cobaltates, we investigate the properties of strong electron correlation on a triangular lattice. Of particular interest is the nature of the Mott transition at half filling on such a lattice. A triangular lattice offers an ideal playground for exploring the Mott transition as a result of the inherent magnetic frustration that is present. We find that a critical value of $U=5.7t$ separates the paramagnetic, insulating and metallic phases. Away from half filling we find a metallic phase characterized by a large Fermi surface on the electron-doped side, as observed experimentally, and a strongly correlated metal with a low-energy physics controlled by a quasidispersionless band on the hole-doped side.

The paper is organized in three main sections. In Sec. II we give an overview of the computational scheme, the cluster dynamical mean-field theory with the noncrossing approximation (NCA) as the impurity solver in the context of the one-band Hubbard model. In Sec. III we discuss the two main issues related to the consistency of the method: the proper periodization procedure to obtain physically meaningful lattice quantities and the cluster size dependence of the results. We show that, for a given small cluster size, the method breaks down at certain filling values, and we argue that the cluster size independence should be the ultimate consistency criterion. In Sec. IV we present the results of the simulations. In Sec. IV A, we show the existence of a quasidispersionless low-energy band, which is a signature of strong correlations and is incompatible with standard Fermi-liquid physics. In Sec. IV B, we discuss the Mott transition on the triangular lattice. Finally, in Sec. IV C, we argue for the existence of a pseudogap at low hole doping.

II. DESCRIPTION OF THE METHOD

We start with the one-band Hubbard model,

$$H = -t \sum_{\sigma,\langle i,j\rangle} c_{i\sigma}^{\dagger} c_{j\sigma} + \text{c.c.} + U \sum_{i} n_{i\downarrow} n_{i\uparrow}, \tag{1}$$

where t is the matrix element for hopping between nearest-neighbor sites, $\langle i,j\rangle$, and U is the on-site repulsive interaction. We assume that the single-band Hubbard model on a triangular lattice captures the main features of strongly correlated physics in the presence of magnetic frustration. We restrict our study to the paramagnetic state,

$$\langle n_{i\downarrow}\rangle = \langle n_{i\uparrow}\rangle = n/2, \tag{2}$$

which is consistent with the experimental observations in cobaltates for $x < 0.5$.

As a computational tool, we use in our investigation a real-space cluster generalization of DMFT.[12] The DMFT has been a very successful tool in investigating many aspects of strongly correlated systems. In this method one single site is treated as an impurity embedded in an effective bath consisting of the rest of the sites the properties of which are captured by the hybridization function. It is exact in infinite dimensions or more precisely in infinite coordination number z, and it can successfully describe the antiferromagnetic order. However for many applications it is necessary for the short-range (few lattice site) correlation to be described accurately. In the cluster DMFT method (CDMFT),[13] a cluster extending in a small number of sites is treated as the impurity and therefore the local (cluster) degrees of freedom are treated exactly. The rest of the lattice, the bath, is described by a multicomponent hybridization function.

All cluster-DMFT-based algorithms contain the following major components:

(i) An impurity solver, which evaluates the cluster Green function from the hybridization function.

(ii) A self-consistency condition which expresses the hybridization function with respect to the cluster Green function.

(iii) A periodization procedure which connects the lattice quantities with the cluster quantities.

A. Impurity solver

The impurity solver evaluates the cluster Green function, given the "external" hybridization function. Various impurity solvers have been proposed in the literature such as exact diagonalization (ED) and quantum Monte Carlo. However the former suffers from poor frequency resolution due to the size of the effective bath and the latter can only be implemented in imaginary time and an analytic continuation is required to obtain real time properties. A real time impurity solver with good frequency resolution is the NCA, which is a first-order perturbation theory with respect to the hybridization function. The pictures that one obtains from using different impurity solvers are somehow complementary. To obtain a more complete description of the Mott physics, a comparison between results obtained with various approaches is necessary. It has the advantage of being very fast and relatively easy to implement. The NCA has been a valuable tool for extracting the physics of the Anderson impurity models. The NCA equations can be obtained by using the slave boson method,[14] and they can be expressed with respect to the pseudoparticle resolvents G_{mn} and their self-energies Σ_{mn}, where m,n are the indices representing the eigenstates of the cluster. The NCA equations, which are used to evaluate the updated resolvent self-energies along with the cluster Green function $G_{\mu\nu}$ for a given hybridization function $\Delta_{\mu\nu}$, are[15]

$$\begin{aligned}\Sigma_{mn}(i\omega) = & \sum_{m'n'\mu\nu} F_{\nu}^{mm'} (F_{\mu}^{n'n})^{*} \\ & \times \int d\xi f(\xi) \Delta_{\mu\nu}(\xi) G_{m'n'}(i\omega + \xi) \\ & + \sum_{m'n'\mu\nu} (F_{\nu}^{mm'})^{*} F_{\mu}^{n'n} \\ & \times \int d\xi f(-\xi) \Delta_{\mu\nu}(\xi) G_{m'n'}(i\omega - \xi),\end{aligned} \tag{3}$$

$$\begin{aligned}G_{\mu\nu}(i\omega) = & -\frac{1}{Q} \sum_{mnm'n'} F_{\mu}^{n'n} (F_{\nu}^{m'm})^{*} \\ & \times \int \frac{d\xi}{\pi} e^{-\beta\xi} [\bar{G}_{m'n'}(\xi) G_{nm}(\xi + i\omega) \\ & - G_{m'n'}(\xi - i\omega) \bar{G}_{nm}(\xi)],\end{aligned}$$

$$Q = -\int \frac{d\xi}{\pi} e^{-\beta\xi} \sum_{m} \bar{G}_{mm}(\xi). \tag{4}$$

The Greek indices correspond to cluster degrees of freedom (site and spin), $F_{\nu}^{mm'} = \langle m | c_{\nu} | m' \rangle$ are the matrix elements of the destruction operator and $f(\xi)$ is the Fermi function. The resolvents can be obtained from the self-energy using the Dyson equation,

$$G_{mn}(i\omega) = [(i\omega - \lambda)\mathbf{1} - \mathbf{E} - \mathbf{\Sigma}]^{-1}_{mn}, \tag{5}$$

where E is the diagonal matrix of the clusters eigenenergies and λ, an artifact of the slave-boson approach, is chosen for convenience.

In the paramagnetic disordered state, both the spin and the irreducible representation of the geometrical symmetry group are good quantum numbers and can be used to label the cluster eigenstates,

$$|m\rangle = |N, S^2, S_z, r, r_m, E\rangle, \tag{6}$$

where r and r_m denote the irreducible representation, and it's row, respectively, and the rest follow standard notation. All but the energy E are good quantum numbers, and they cannot be affected by the bath. Furthermore all resolvents with the same N, S^2, r but different S_z and r_m are the equal to one another.

B. Self-consistency condition

The self-consistency condition generates a new hybridization function, i.e., a new effective environment for the impurity cluster, starting from a given cluster Green function $G_{\mu\nu}$ and taking into account the geometry of the lattice and the noninteracting hopping matrix. Within the CDMFT scheme, the self-consistency condition reads

$$\sum_{\mathbf{K}} [\mathbf{M}^{-1} - \mathbf{E}(\mathbf{K})]^{-1} = (\mathbf{M}^{-1} - \mathbf{\Delta} - \mathbf{T}_0)^{-1}, \tag{7}$$

where the matrix $\mathbf{E}(\mathbf{K})$ is the Fourier transform of the intercluster hopping matrix $\mathbf{T}_{IJ}$, with I and J being indices that label the clusters inside the superlattice and $\mathbf{K}$ is the superlattice momentum. The cluster cumulant $M_{\alpha\beta}$ can be expressed in terms of the intracluster hopping matrix $\mathbf{T}_0 = \mathbf{T}_{II}$ as

$$\mathbf{M}^{-1} = \mathbf{G}^{-1} + \mathbf{\Delta} + \mathbf{T}_0. \tag{8}$$

C. Lattice periodization

Once the cluster quantities such as the cumulant or the self-energy have been obtained, the corresponding lattice quantities need to be reconstructed.[16] A good estimate of these lattice quantities can be obtained by averaging over all the possible ways in which a lattice can be covered with clusters of a given type. For each type of cluster and each lattice there are a finite number, N_S, of different realizations of the superlattice, which are related to one another by a symmetry operation (rotation, translation, or both). Explicitly, a lattice quantity $X_{\text{latt}}(\mathbf{x}_\alpha - \mathbf{x}_\beta)$, which may be either the cumulant of the self-energy, can be extracted from the corresponding set of cluster components $X(\mathbf{x}_\alpha, \mathbf{x}_\beta)$ as

$$X_{\text{latt}}(\mathbf{x}_\alpha - \mathbf{x}_\beta) = \frac{1}{N_S} \sum_S X^{\text{SL}}(S[\mathbf{x}_\alpha], S[\mathbf{x}_\beta]), \tag{9}$$

where X^{SL} represents the quantity X for a certain reference superlattice, S is a symmetry operation relating different equivalent superlattices to the reference superlattice, and $S[\mathbf{x}_\alpha]$ is the new position of site $\mathbf{x}_\alpha$ after applying the symmetry operation. If the positions $S[\mathbf{x}_\alpha]$ and $S[\mathbf{x}_\beta]$ do not belong to the same cell of the reference superlattice $X^{\text{SL}}(S[\mathbf{x}_\alpha], S[\mathbf{x}_\beta])$ vanishes; otherwise it is given by the corresponding cluster component. The momentum dependence is obtained by a simple Fourier transform,

$$X_P(\mathbf{k}) = \sum_\beta X_{\text{latt}}(\mathbf{x}_\alpha - \mathbf{x}_\beta) e^{i(\mathbf{x}_\alpha - \mathbf{x}_\beta)\cdot\mathbf{k}}, \tag{10}$$

where the index P signifies that the quantity $X(\mathbf{k})$ was obtained by applying the periodization procedure.

In this paper, we focus on the cumulant periodization scheme $X \equiv M$, in which the lattice Green function is given by

$$G_{\text{latt}}(\omega, \mathbf{k}) = \frac{1}{M_P^{-1}(\omega, \mathbf{k}) - \epsilon(\mathbf{k})}. \tag{11}$$

We also discuss briefly the implications of using the self-energy periodization scheme. Note that the cluster self-energy is related to the cluster cumulant through the matrix equation,

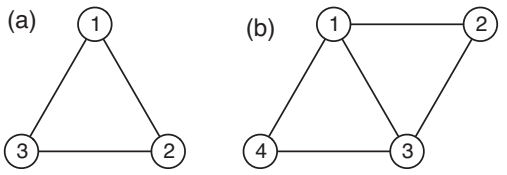

FIG. 1. Types of clusters used in the simulation: (a) triangle and (b) rhomboid.

$$\mathbf{\Sigma} = (\omega + \mu)\mathbf{1} - \mathbf{M}^{-1}, \tag{12}$$

and a similar scalar equation holds for the corresponding lattice quantities, $\Sigma(\mathbf{k}) = (\omega + \mu) - M(\mathbf{k})^{-1}$. In this scheme the lattice Green function is given by

$$G_{\text{latt}}(\omega, \mathbf{k}) = \frac{1}{\omega + \mu - \epsilon(\mathbf{k}) - \Sigma_P(\omega\,.\,\mathbf{k})} = \frac{1}{(M^{-1})_P(\omega, \mathbf{k}) - \epsilon(\mathbf{k})}, \tag{13}$$

where the index P implies that M^{-1} is periodized.

In this paper we are going to use two types of clusters: a triangular three-site cluster and a rhombic four-site cluster (Fig. 1). Because of paramagnetism and also the geometrical symmetry, the triangular cluster has 31 independent resolvents and 2 independent cluster quantities, whereas the rhombic cluster has 309 and 5, respectively. Single-site and two-site clusters have also been considered but convergence is possible only at higher temperatures. The respective superlattices are shown in Fig. 2.

For the triangular cluster, there are only two independent components, a local X_0 and the nearest-neighbor one X_1. The corresponding periodization is

$$X_{\text{tri}}(\mathbf{k}) = X_0 + 2X_1 a(\mathbf{k}),$$

where $a(\mathbf{k}) = \frac{1}{3}\Sigma_{i=1}^3 \cos k_i$ and $k_1 = k_x$, $k_2 = -\frac{1}{2}k_x + \frac{\sqrt{3}}{2}k_y$, and $k_3 = -\frac{1}{2}k_x - \frac{\sqrt{3}}{2}k_y$. For the rhombic cluster there are five independent components: two local ones, X_0 and X_0', corresponding to the site with three and two neighbors inside the cluster, respectively, two nearest-neighbors, X_1 and X_1', corresponding to one of the sides of the cluster and the diagonal link, respectively, and one next-to-nearest-neighbor component X_2 along the long diagonal of the cluster. The periodization is

$$X_{\text{rho}}(\mathbf{k}) = \frac{X_1 + X_2'}{2} + \left(2X_1 + \frac{1}{2}X_1'\right) a(\mathbf{k}) + \frac{X_2}{2} b(\mathbf{k}),$$

where $b(\mathbf{k}) = \frac{1}{3}\Sigma_{i=1}^3 \cos(k_i - k_{i+1})$, with $k_4 = k_1$. Since a uniform paramagnetic phase is assumed, the choice of the cluster is expected to have a relatively small impact on the physical quantities for regimes characterized by short correlation lengths.

III. NUMERICAL SCHEME: CONSISTENCY, OPTIMIZATION, AND LIMITATIONS

The key feature that makes a DMFT-type treatment applicable is the locality of the correlated physics. In infinite di-

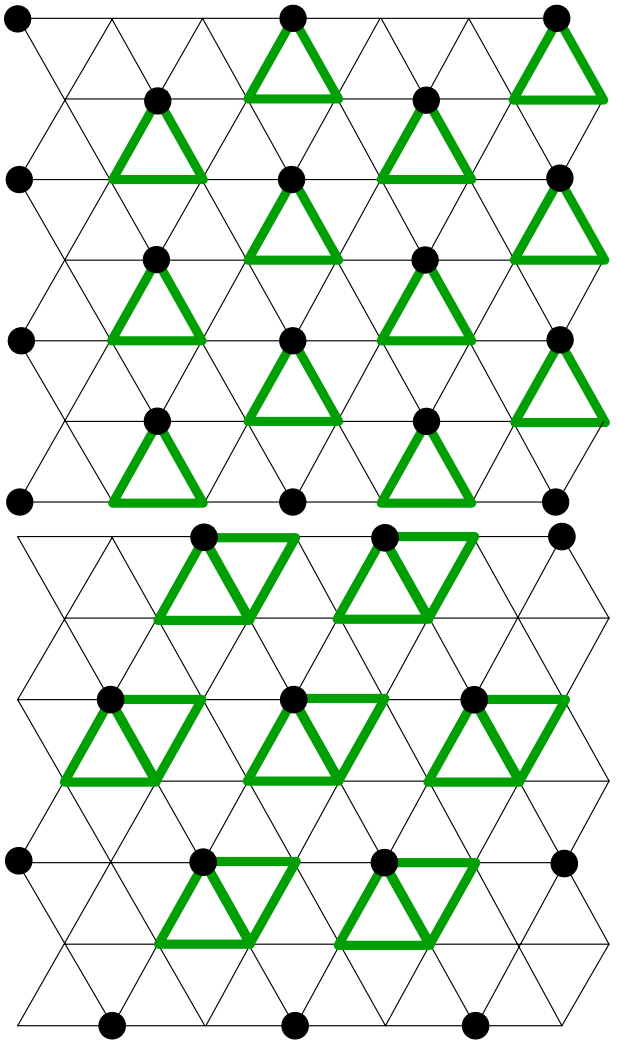

FIG. 2. (Color online) Triangular (left) and rhomboid (right) cluster's superlattices. The black circles represent the superlattice's sites.

mensions, the correlations are purely local and can be described by a momentum-independent self-energy. In finite dimensions, the basic assumption is that the correlations are short ranged and can be captured by a cluster extension of DMFT. The size of the cluster that would properly capture the physics is determined by the range of the relevant correlations and cannot be known *a priori*. Therefore, consistency checks are a necessary component of any cluster DMFT treatment. In this section, we show that for the two-dimensional Hubbard model on a triangular lattice: (A) The self-energy is not a short-range quantity in the vicinity of the Mott insulating phase and therefore should not be extracted from the cluster components. Instead, the renormalized two-point cumulant satisfies the locality requirement and can be used for reconstructing the lattice quantities. (B) A cluster scheme does not work equally well for all doping values. In particular, for certain doping levels commensurate with the cluster size the scheme predicts spurious "insulating" states. We argue that a comparison between results obtained using clusters of different sizes is crucial. The ultimate consistency

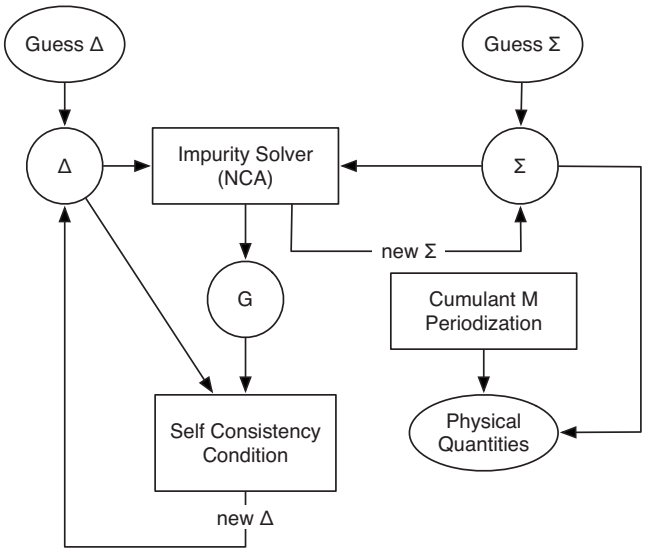

FIG. 3. Flow diagram for the CDMFT+NCA method. $\mathbf{\Delta}$ is the bath function, $\mathbf{\Sigma}$ is the resolvent self–energy, and $\mathbf{G}$ is the cluster Green function, and the cumulant is $\mathbf{M}=\mathbf{G}^{-1}+\mathbf{\Delta}+\mathbf{T}_0$. The flow starts at the guesses of $\mathbf{\Delta}$ (usually with a Gaussian imaginary part) and $\mathbf{\Sigma}$ (negative imaginary constant). The impurity solver evaluates a new $\mathbf{\Sigma}$ from $\mathbf{\Delta}$ and the old $\mathbf{\Sigma}$ and also the cluster Green function. The self-consistency condition takes as its input the cluster Green function and the old $\mathbf{\Delta}$ to return an updated $\mathbf{\Delta}$. The impurity solver and self-consistency condition iterate until convergence is reached. Then the cumulant $\mathbf{M}$ is evaluated and periodized. Physical quantities can be obtained from $\mathbf{M}$ (for example, the spectral function) and $\mathbf{\Sigma}$.

criterion is the invariance of results to an increase of the cluster size.

To solve for the cluster quantities and the resolvents self-consistently, we start from an initial guess for the imaginary part of the resolvent self-energies and the hybridization function. The real part was obtained through the Krammers-Kronig relationships. One possibility is to start at high temperatures ($T \approx 0.3t$) where the method converges very easily (a constant $\Im\Sigma_{mn}$ and a Gaussian $\Im\Delta_{\mu\nu}$ is enough) and then "cool down" progressively using in every step the solution of the previous step. Usually a two-step process suffices. Once the initial guess is obtained, the NCA equations [Eqs. (3) and (4)] along with Eq. (5) are used to update Σ_{mn} and evaluate the cluster Green function $G_{\mu\nu}$. From the latter and the self-consistency condition [Eq. (7)] the hybridization function $\Delta_{\mu\nu}$ is updated. The process iterates until convergence is reached. The lattice Green function and the corresponding spectral function are obtained by the periodized cumulant. A flow diagram of the process is shown in Fig. 3. From the spectral function, a variety of two-particle properties can be obtained.

A. Cumulant vs self-energy periodization

Our first task is to test the accuracy of the periodization procedure and identify the quantity most suitable to be used in the periodization scheme. Note that the implicit physical assumption behind periodizing a certain quantity $X(\mathbf{x}_\alpha, \mathbf{x}_\beta)$ is

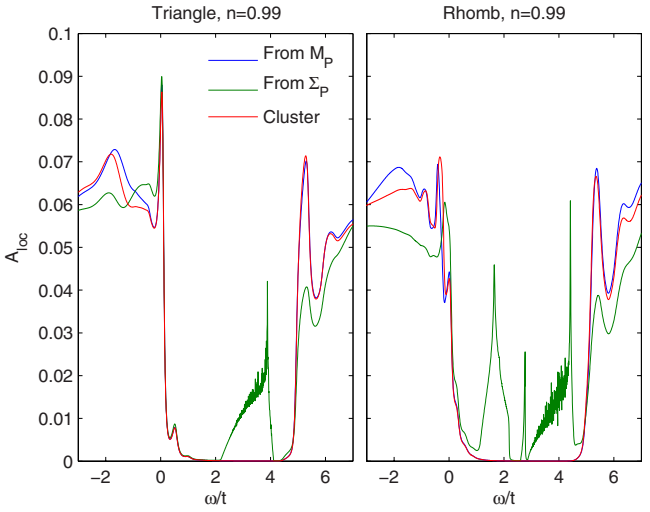

FIG. 4. (Color online) Comparison of the density of states for the cumulant and self-energy periodization for the triangular cluster at $U=12t$ and $T=0.1t$.

the short-range nature of that quantity. A long-range quantity cannot be properly approximated in any way using finite range cluster components.

To chose the proper periodization procedure, we compare the density of states (DOS) for cumulant and self-energy periodization for both three-site and four-site clusters. In the vicinity of half filling, regardless of the cluster size, the self-energy periodization results in states lying inside the Mott gap, as shown in Figs. 4 and 5. These states are clearly unphysical, as demonstrated by the comparison with the local cluster spectral function, which shows a well-defined clean Mott gap, as shown in Fig. 6. On the other hand, these midgap states are absent in the cumulant periodization procedure. This signals that the cumulant is a short-range quantity in the vicinity of the Mott transition, while the self-energy is not, but contains long-range components that cannot be captured with a small size cluster.[17]

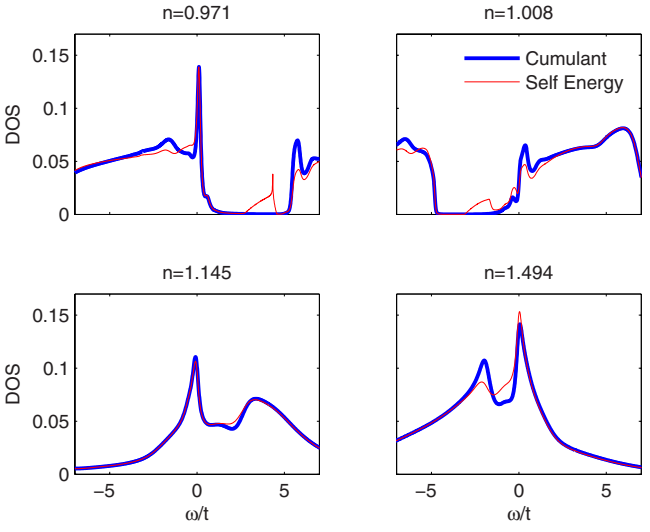

FIG. 5. (Color online) Comparison of the density of states for the cumulant and self-energy periodization for rhombic cluster at $U=12t$ and $T=0.1t$.

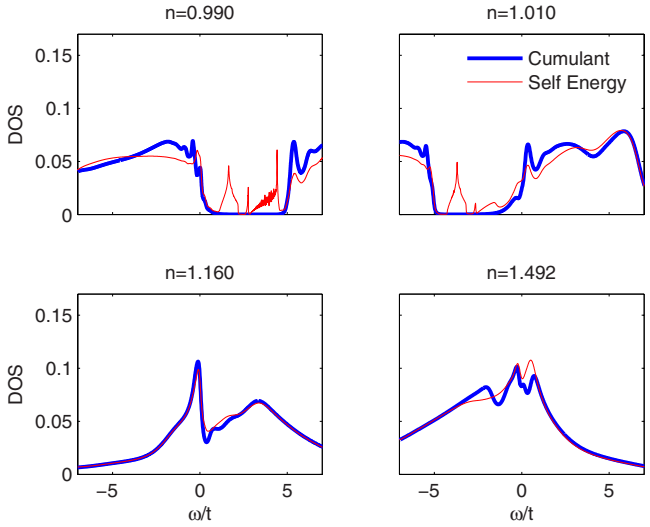

FIG. 6. (Color online) Comparison of the local cluster spectral function, A_{ii}, with the one obtained through cumulant M_P and self-energy Σ_P periodization for the triangular (left) and rhombic clusters (right) at $U=12t$ and $T=0.1t$. The local cluster spectral function agrees with that from M_P. The one obtained from Σ_P predicts unphysical states in the middle of the Mott gap.

In contrast, at large dopings in the Fermi-liquid phase, where both the self-energy and the cumulant are short-range quantities, the two methods agree. We conclude that the self-energy periodization is appropriate away from the Mott transition, while the cumulant scheme gives consistent results in a wide range of dopings. In the present study we will use the cumulant method regardless of filling. The reason for the failure of the self-energy periodization method is the presence in the half-filled regime of self-energy divergences[16,18] at $\omega=0$ and low temperatures. This divergence of the self-energy at half filling is intimately linked to the Mott gap.

B. Commensurate insulators

Away from half filling, for certain doping values, there is a substantial discrepancy between the two clusters. Explicitly, our method predicts that around $n\approx 1.25$ for the rhombic cluster and $n\approx 1.33$ for the triangular cluster, the system becomes an insulator, as evidenced by the gap in the density of states in Figs. 7(a) and 7(b), respectively. Note that it is very hard to obtain convergence with NCA whenever there is a sizable gap at the Fermi level, especially for the rhombic cluster. In this case we have to either increase the temperature or slightly change the filling so that the gap becomes partially filled. For this reason we choose $n\approx 1.22$ as shown in Fig. 7(a).

To better understand the commensurate insulator phases, we can analyze the resolvents within NCA and evaluate the contribution of each cluster state. It is therefore possible to determine which are the dominant channels through which the cluster interacts with the bath. The relevant quantity is the partial occupancy of a particular cluster state,

$$\langle n_{mm}\rangle = -\frac{1}{Q}\int \frac{d\xi}{\pi} e^{-\beta\xi} n_{mm}\bar{G}_{mm}(\xi). \qquad (14)$$

Small occupancy signifies that the corresponding resolvent contributes insignificantly to the cluster spectral function and

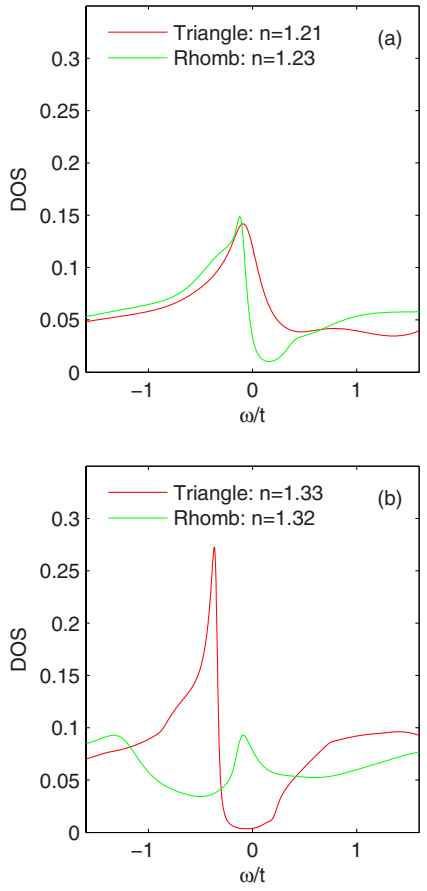

FIG. 7. (Color online) The density of states for both clusters for (a) $n \approx 1.22$ and (b) $n \approx 1.33$.

consequently to the hybridization function. Therefore, the resolvents with small occupancy can be ignored, whereas the ones with large overlap have the dominant contribution to the dynamics of the system. For the triangular cluster it turns that there are only seven resolvents with an overlap larger than 0.01, whereas the rest have occupancy less than 0.0025. A similar analysis can be performed for the rhombic cluster. As expected there are more resolvents with substantial occupancy. In Fig. 8 only the dominant ones are plotted which have occupancy more than 0.1. Their quantum numbers are shown in Table I. In all cases, we observe that when the dominant resolvents have fillings i/N_c close to the lattice filling, their partial occupancy peaks and transitions from and to them become rare, which gives rise to an insulating state. In the triangular lattice this has a consequence when $n=4/3$ because in this case there is only one dominant resolvent. As a result, there is no appreciable overlap with any electronic states, leading thereby to a gap in the spectrum. In the rhombic cluster, around the critical value $n=5/4$ there are two dominant resolvents which means that even though the transitions are limited, a gap still persists although it is not as pronounced as in the three-site cluster. We have also obtained commensurate insulating states for fillings $n=2/3$, for the triangular and $n=3/4$, for the rhombic cluster, but in this regime convergence is not reached at low temperature. The presence of such insulating states ultimately points to a limitation of the finite cluster approach to the Hubbard model.

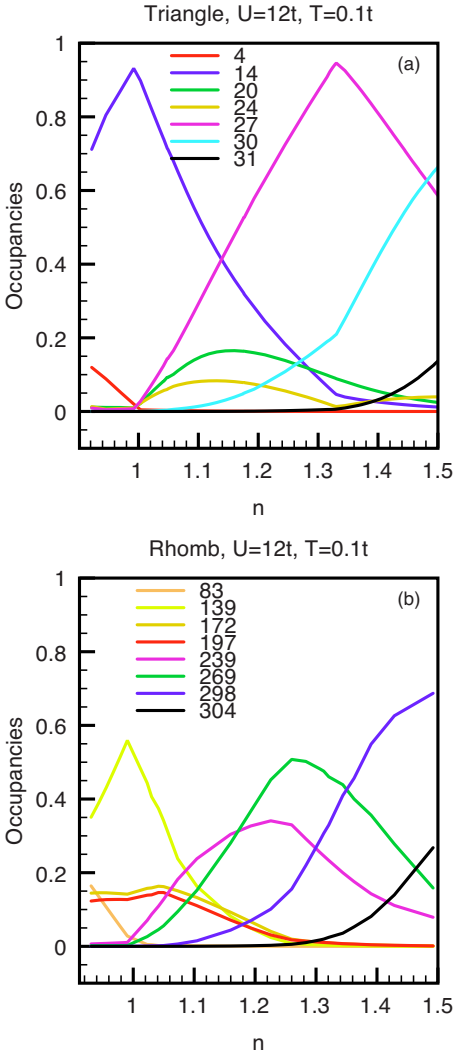

FIG. 8. (Color online) The occupancies $\langle n_{mm} \rangle$ as a function filling for the dominant resolvents in the (a) triangular and (b) rhombic clusters.

We emphasize that the appearance of the fictitious commensurate insulating states is a consequence of using small clusters in the numerical calculations. In all the present implementations of the CDMFT cluster methods for finite dimensions higher than one, there is always a difficulty related to the fact that most or all of the cluster sites lie on the cluster boundaries. To address this large size cluster studies are necessary in order to clarify all aspects of Mott physics on the triangular lattice. However, before dealing with the numerical difficulties of using large clusters, progress can also be made by making small cluster comparisons for the following reasons: (a) to show explicitly that some aspects of the Mott physics in two dimensions are different than their infinite dimension counterparts and also differ between the square and the triangular lattice geometries and (b) to give an estimate of the systematic errors inherent in the finite cluster size methods. Since DMFT does not provide a small parameter to control the accuracy, we argue that information about this accuracy can be extracted by varying the cluster size. Furthermore, features that are independent of the cluster size can be attribute to the underlying lattice physics. For ex-

TABLE I. The quantum numbers of the dominant resolvents for the rhombic cluster for $U=12t$ and $T=0.1t$. Their occupancy is shown in the left panel of Fig. 8. The quantum numbers are explained in the legend of Table II.

Label	N	S^2	S_z	r	r_m	E
83	3	1/2	1/2	$B_1;x$	1	−3.07
139	4	0	0	$B_1;z$	1	−0.94
172	4	1	1	$B_1;z$	1	−0.67
197	4	1	1	$B_1;x$	1	−0.65
239	5	1/2	1/2	$B_1;y$	1	9.39
269	5	3/2	3/2	$B_1;z$	1	9.44
297	6	1	1	$B_1;y$	1	21.44
304	7	1/2	1/2	A_1	1	34.44

ample, the existence and the properties of the Mott insulating phase at half filling, $n=3/3=4/4$, can be obtained consistently using various cluster sizes. Moreover, as the on-site interaction U is reduced, a transition to a metallic state is consistently observed, with some small cluster size dependence of the critical parameters.

IV. RESULTS

In this section we present our main results. In Sec. IV A, we show that the two-dimensional Hubbard model on a triangular lattice is a strongly correlated system by demonstrating that the low-energy physics is controlled by a weakly dispersing band with spectral weight that can be transferred over large energy scales. Section IV B is devoted to the characterization of the interaction-controlled Mott metal-insulator transition at half filling. In contrast to the infinite dimensional case when a coherence peak develops inside the Mott gap, we find that the insulator-metal transition is characterized by the complete collapse of the Mott gap followed by the appearance of a small peak in the density of states. Finally, in Sec. IV C we investigate the system at low dopings and discuss a perspective on pseudogap physics. We argue that the pseudogap should not be simply identified by the depletion of the density of states at the chemical potential but rather by the change in the location of the low-energy modes in momentum space as compared with the noninteracting system. According to this picture, the pseudogap phase is essentially characterized by a reconstructed Fermi surface consisting of small pockets that vanish in the zero doping limit.

A. Dispersionless low-energy band

The main figure and the inset in Figs. 9 and 10 reveal a lack of particle-hole symmetry for electron and hole dopings. This is expected as a triangular lattice does not preserve this symmetry. While the asymmetry persists regardless of the cluster size, the details differ. Of particular interest is the presence of a dispersionless subband residing near the top of the lower Hubbard band upon hole doping. The occurrence of such a band is inconsistent with Fermi-liquid behavior: the chemical potential crosses the band in an extended area instead of at a well-defined curve. This band occurs in both the triangular and the rhombic clusters; but in the latter it appears split. This splitting, shown not only in Fig. 11 but also in the density of states as shown in Fig. 12, may be due to the higher resolution gained by using the rhombic cluster.

A shadow of this band persists unsplit and with less spectral weight even in the electron-doped regime where the system is a normal metal, as shown in Fig. 13. Therefore the splitting is due to the fact that it crosses the chemical potential. Consequently, in the triangular lattice, particle hole

TABLE II. The quantum numbers corresponding to the dominant resolvents for the triangular cluster for $U=12t$, $T=0.1t$. Their occupancy is shown in the left panel of Fig. 8. The quantum numbers are the particle number N, the spins S^2 and S_z, the label of the irreducible r and the corresponding row r_m (Ref. 35), and the eigenenergy E.

Label	N	S^2	S_z	r	r_m	E
4	2	0	0	A_1	1	−2.55
14	3	1/2	1/2	$E;x,y$	1	−0.50
20	3	3/2	3/2	$A_2;z$	1	0.00
24	4	0	0	A_1	1	10.85
27	4	1	1	$A_2;z$	1	10.00
30	5	1/2	1/2	$E;x,y$	1	23.00
31	6	0	0	A_1	1	36.00

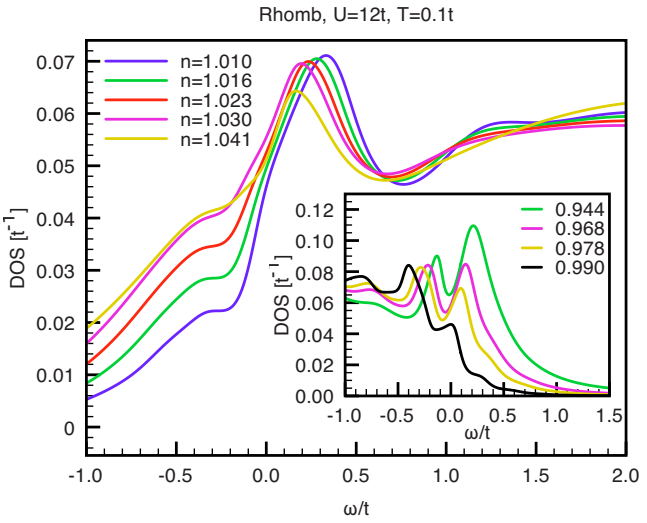

FIG. 9. (Color online) The evolution of the density of states as a function of doping in the upper and lower (inset) Hubbard bands.

asymmetry gives rise to a non-Fermi-liquid behavior for hole doping and metallic behavior (Fig. 13) in the electron-doped side. This band structure can be compared with experimental results.[19] A full comparison is not possible because only one band, namely, the a_{1g} is taken into account and the $e_{g'}$ is ignored. However the experiment shows the existence of an almost flat band with energy −0.6 eV. The present calculation is evidence that this band may emerge purely because of strong correlations. Further evidence that this band arises from purely strong electron correlations comes from the fact that it is absent in local-density approximation (LDA) and linear augmented plane-wave (LAPW) calculations [Fig. 3 of Ref. 19].

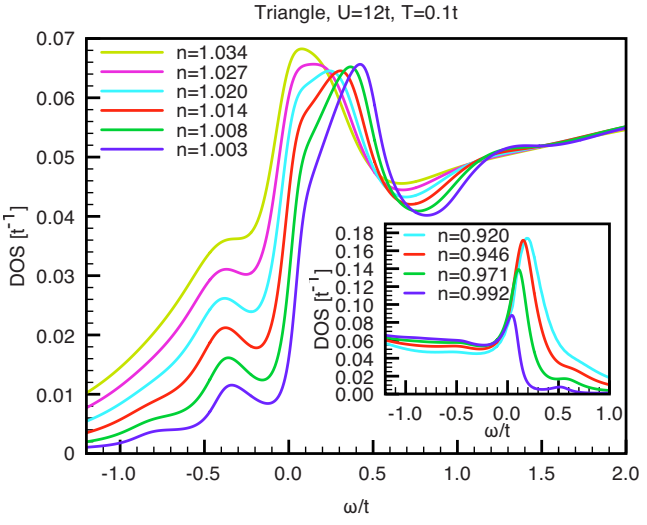

FIG. 10. (Color online) Evolution of the density of states for the triangular cluster around half filling for $T=0.1t$ and $U=12t$ in the electron-doped regime (upper Hubbard band). There is a pseudogap feature which does not align with the chemical potential ($\omega=0$) and which disappears for a doping of $n=3.5\%$. The inset shows the density of states in the hole-doped regime (lower Hubbard band), which exhibits no pseudogap feature.

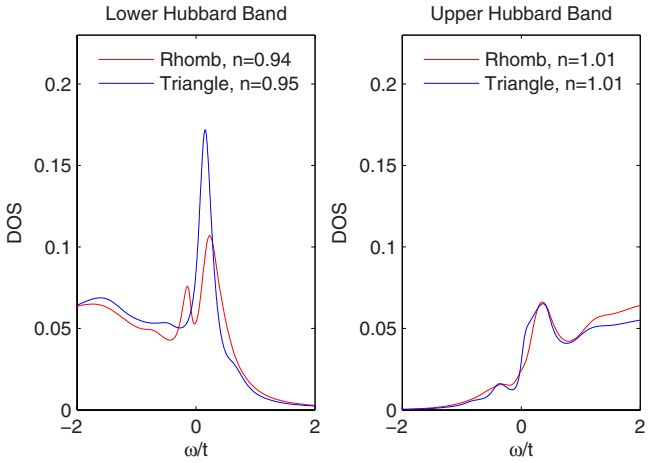

FIG. 11. (Color online) Comparison of the density of states between the rhombic and the triangular clusters in the upper and lower Hubbard bands. There is good agreement in the electron-doped regime. In the hole-doped regime there is a dispersionless band which the rhombic clusters resolves as being split.

B. Mott transition

The density of states for high enough U exhibits an interaction-induced gap around half filling, as shown in Fig. 14. Clearly shown in Fig. 14 is the closing of the gap between the lower and upper Hubbard bands as the on-site interaction decreases, indicative of a Mott transition. To pinpoint the precise location of the Mott transition, we estimate the Mott gap by the discontinuity, $\Delta\mu$, in the chemical po-

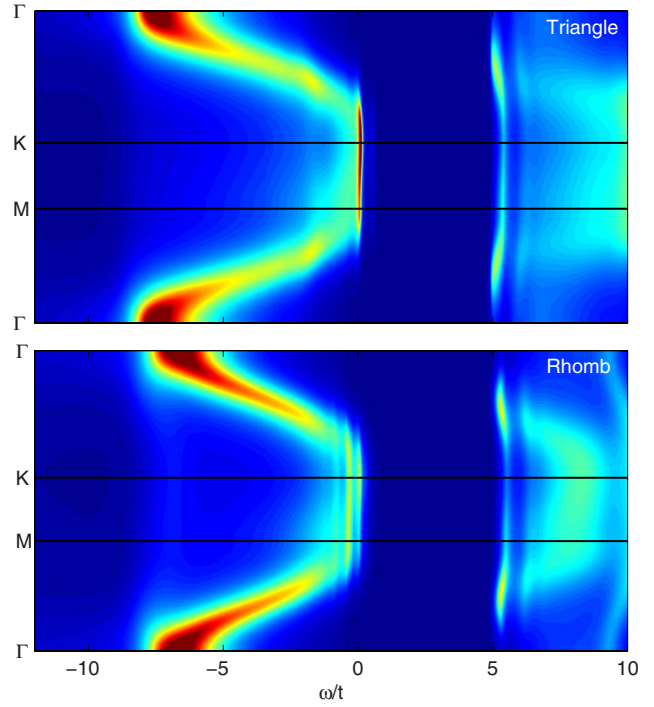

FIG. 12. (Color online) The spectral function as a function of k and ω for $U=12t$, $T=0.1t$, and $n=0.99$. Upper panel: triangular cluster. Lower panel: rhombic cluster. Both methods give a dispersionless band, but in the rhombic cluster it is resolved in two.

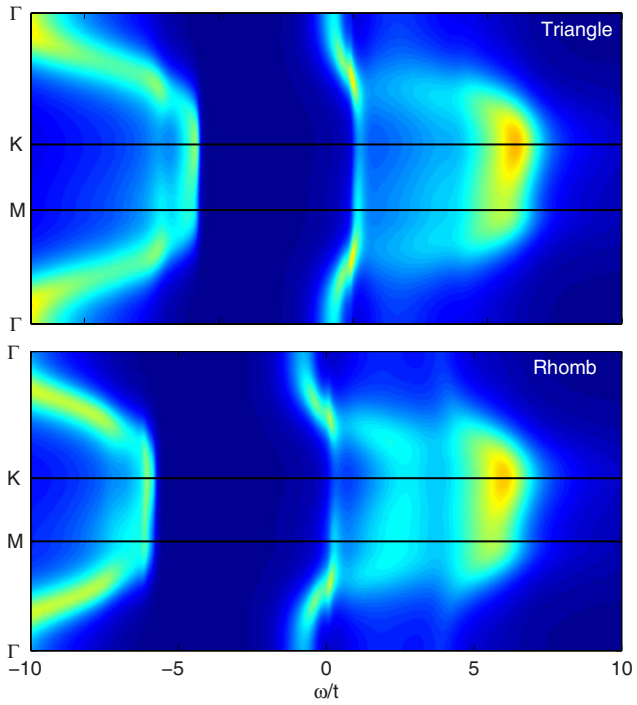

FIG. 13. (Color online) Spectral function for $U=12t$, $T=0.1t$, and $n=1.04$ for the triangular (upper panel) and rhombic clusters (lower panel). The chemical potential crosses a narrow band, and the behavior is metallic. The dispersionless subband at the top of the lower Hubbard band persists but with less spectral weight and unsplit.

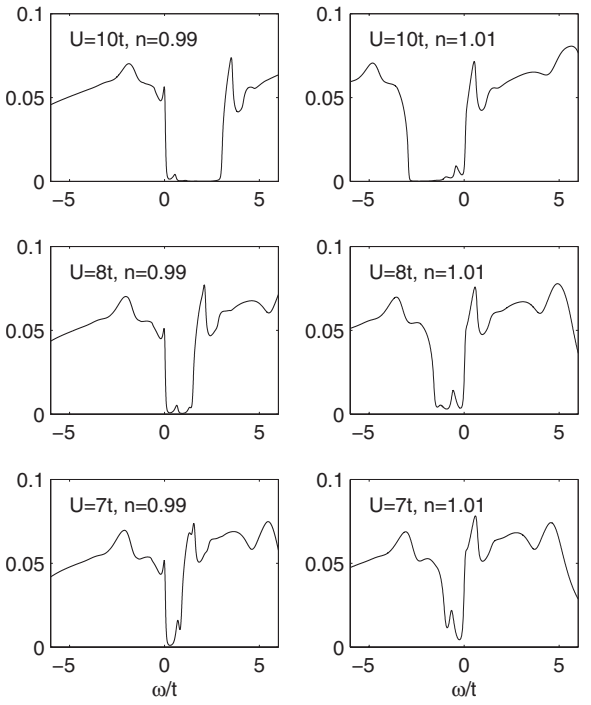

FIG. 14. The density of states in units of t^{-1} in the vicinity of half filling for the triangular cluster. The gap closes with decreasing U.

tential on either side of half filling. Figure 15 displays a typical calculation of the chemical potential as a function of the filling for both three-site and four-site clusters. Because of thermal broadening, this procedure would underestimate $\Delta\mu$, which cannot discriminate below energy scales of the order of kT. For both cluster sizes, the results are consistent yielding a gap of $\Delta\mu \approx 5t$ for $U=12t$. As the inset demonstrates, the discontinuity in the chemical potential across half filling vanishes at $U_c \approx 5.7t$. However, $\Delta\mu$ provides only a rough estimate of the critical U because the precise magnitude of the gap is obscured as shown in Fig. 15. To probe the transition more directly, we plot the density of states for different values of U around the estimate obtained from the chemical-potential analysis. Figure 16 displays clearly that for $U \geq U_c$, with $U_c \approx 5.75t$ and $U_c \approx 4.75t$ for the triangle and rhombic clusters, respectively, the system is an insulator, whereas for $U < U_c$ a Drude peak emerges at the chemical potential. Note that the density of states near the chemical potential remains unchanged (relative to its value for $U > U_c$) although the density of states at the chemical potential develops a nonzero value as a transition is made to a metallic state. Consequently, the states that fill in the Mott gap and give rise to the coherence peak arise from spectral weight transfer from high energy, the essence of Mottness. This is illustrated in Figs. 17 and 18 which compare the spectral function right before and after the transition for the triangular and rhombic clusters, respectively. Such a redistribution of spectral weight far from the chemical potential near the Mott transition has been recently observed in the manganites.[20]

The operative mechanism for the Mott transition in the three-site and four-site cluster analyses stands in contrast to the scenario predicted by DMFT.[12] In this scenario a coherent peak of constant height exists at the chemical potential, which successively narrows as U increases to U_c. For $U > U_c$, the peak vanishes and the upper and lower Hubbard

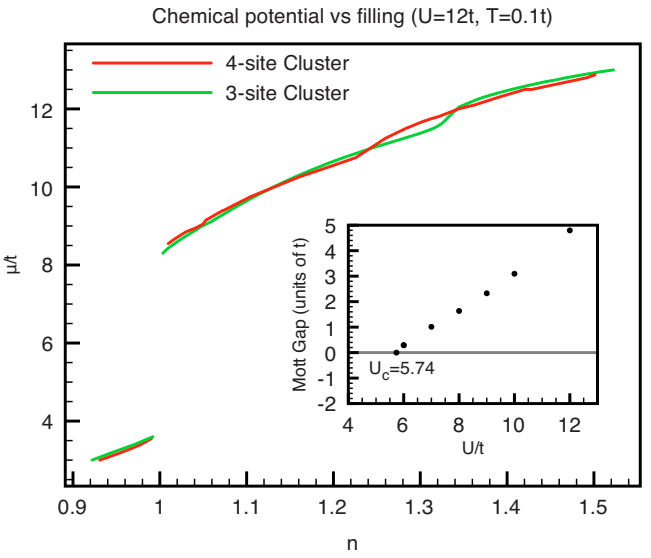

FIG. 15. (Color online) The chemical potential as a function of filling for the three-site and four-site clusters at $U=12t$ and $T=0.1t$. There is agreement anywhere apart from the commensurate fillings $n=4/3$ and $n=5/4$, respectively. Inset: the evolution of the Mott gap as a function of the interaction strength U for the triangular cluster. The gap is linear in U and vanishes at $U_c=5.74t$.

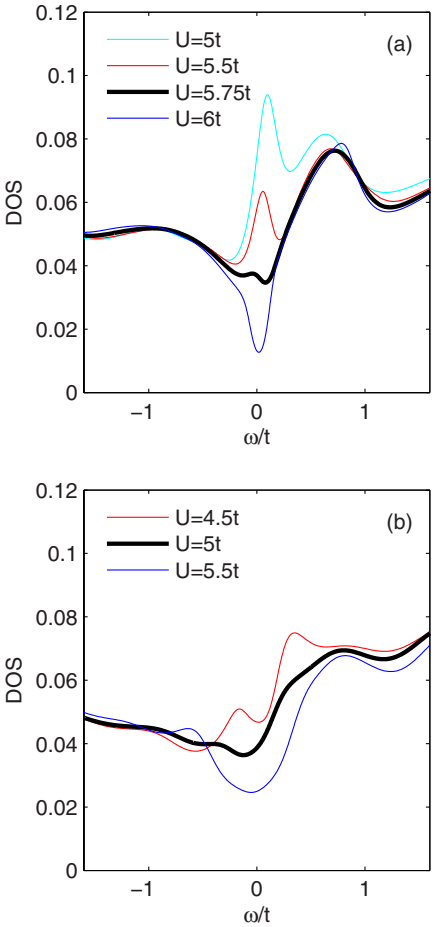

FIG. 16. (Color online) (a) Density of states around the Mott transition for the triangular cluster at $n=1$ and $T=0.1t$. As U decreases, the Drude peak around the chemical potential gradually loses weight until it turns into a gap. The transition occurs at some $U_c \approx 5.75t$. (b) Density of states around the Mott transition for the rhombic cluster at $T=0.12t$, $n=1$, and $U_c \approx 4.5t$.

bands become well separated. CDMFT with exact diagonalization in the square lattice[21] offers a different scenario: first a pseudogap opens at the chemical potential which smoothly grows to form a full Mott gap at the critical U. Therefore a (pseudo)gap always exists in the square lattice, unless frustration, which is described by t', is introduced,[22,23] in which case the gap closes due to the merging of the two bands. In the triangle, there is no formation of a pseudogap. Instead the coherence peak at the chemical potential loses weight Z as U increases and is smoothly replaced by a gap which broadens as the two bands separate. This is consistent with results obtained with CDMFT and ED.[10]

C. Pseudogap

In light of the physics in the cuprates, one of the main questions that needs to be addressed is whether or not a Mott system on a triangular lattice exhibits a pseudogap. We focus here on the single-particle density of states as a function of filling. In the triangular lattice, there is only indirect evidence from a boson analysis of the optical conductivity for a

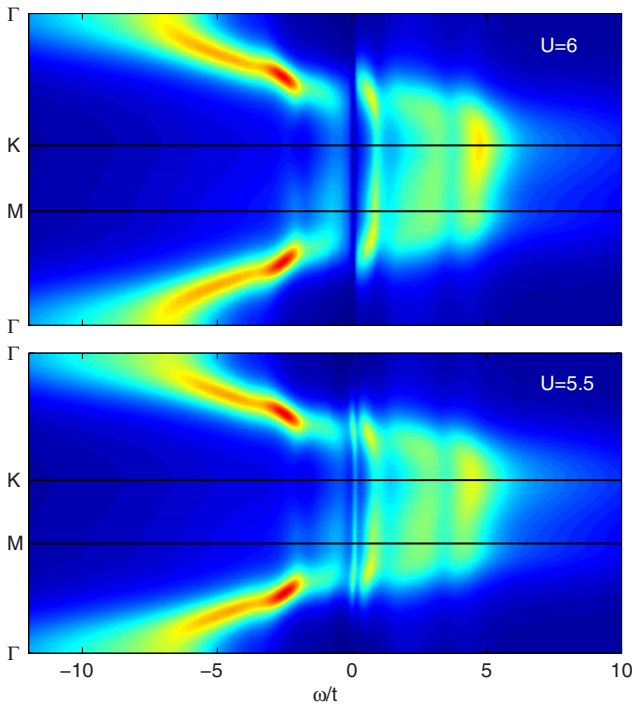

FIG. 17. (Color online) The spectral function at half filling and $T=0.1t$ as a function of ω and k along the $\Gamma \rightarrow K \rightarrow M \rightarrow \Gamma$ path for $U=6t$ (upper panel) and $U=5.5t$ (lower panel) as obtained from the triangular cluster. The spectral weight mostly from energy around $4.5t$ is transferred to the chemical potential during the transition.

pseudogap in the paramagnetic phase ($n<1.5$),[24,25] which disappears in the strange metal phase ($n>1.5$). However numerical simulations suggest otherwise. Results obtained by dynamical cluster approximation with the NCA or fluctuation exchange approximation on an anisotropic triangular lattice[26] suggest the absence of a pseudogap. Instead, with increasing frustration (measured by t'), the frustration due to nonlocal correlations suppresses antiferromagnetic order and gives rise to heavy quasiparticles near half filling, and a pseudogap in the density of states is replaced by a quasiparticle peak at the Fermi level. A similar work[27] on the anisotropic triangular lattice for $t'/t=0.8$ has also shown the emergence of heavy quasiparticles at the Fermi level.

Our results for the single-particle density of states on either side of half filling are summarized in Figs. 9 and 10. Although a diplike features exists for both the three-site and four-site clusters, it is displaced from the chemical potential. For higher dopings, the density of states is smooth in the vicinity of the chemical potential. Consequently, we find an absence of a pseudogap near half filling on a triangular lattice. This result is consistent with the one obtained for the triangular lattice by CDMFT using exact diagonalization calculations as the impurity solver.[10] We traced the origin of the diplike feature to an energy splitting of two resolvents in the triangular lattice (three in the rhombic) with total spin differing by 1. The relevant energy scale is $J=6t^2/U$. To probe this feature further, we calculated its evolution as the temperature is lowered. As is evident from Fig. 19, as the temperature is lowered, the diplike feature remains below the chemical potential and more importantly the peak at the chemical poten-

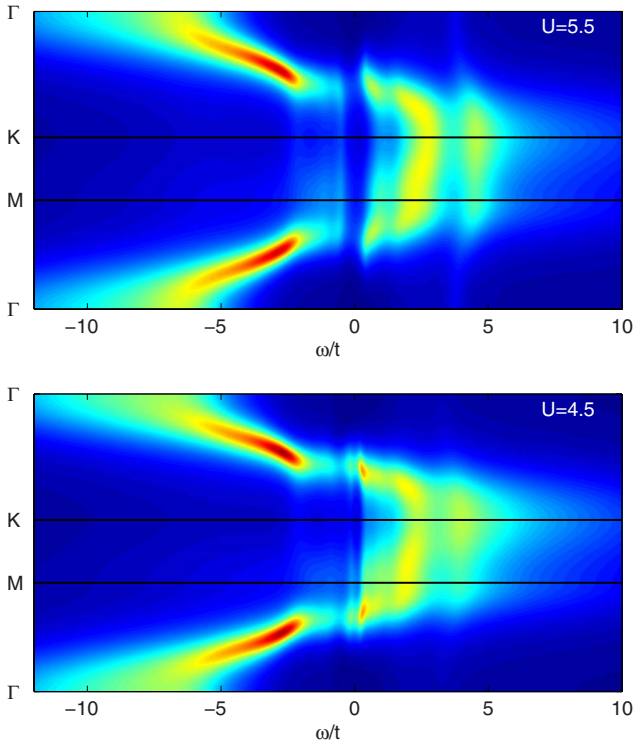

FIG. 18. (Color online) The spectral function at half filling and $T=0.1t$ as a function of ω and k along the $\Gamma \rightarrow K \rightarrow M \rightarrow \Gamma$ path for $U=5.5t$ (upper panel) and $U=4.5t$ (lower panel) as obtained from the rhombic cluster. The spectral weight mostly from energy around $4.5t$ is transferred to the chemical during the transition.

tial sharpens, as would be expected for a metallic state. It has to be noted that in this approximation there is an ambiguity in the determination of the Fermi level or the order of the temperature ($T=0.07t$). However the pseudogap feature develops in frequency $\omega \approx -3T$ which is well away. The metallic behavior is also consistent with the spectral function of the rhombic cluster as shown in Fig. 20. There we see that

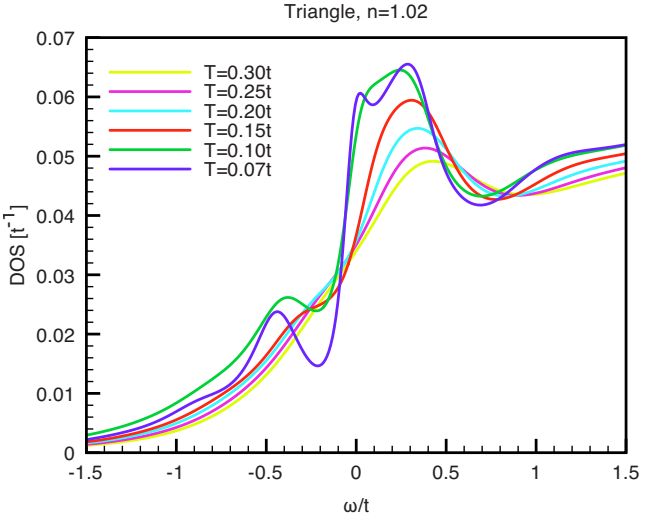

FIG. 19. (Color online) Evolution of the DOS around the chemical potential for $n=1.02$ using the triangular cluster. The pseudogap feature is dispersed as the temperature increases.

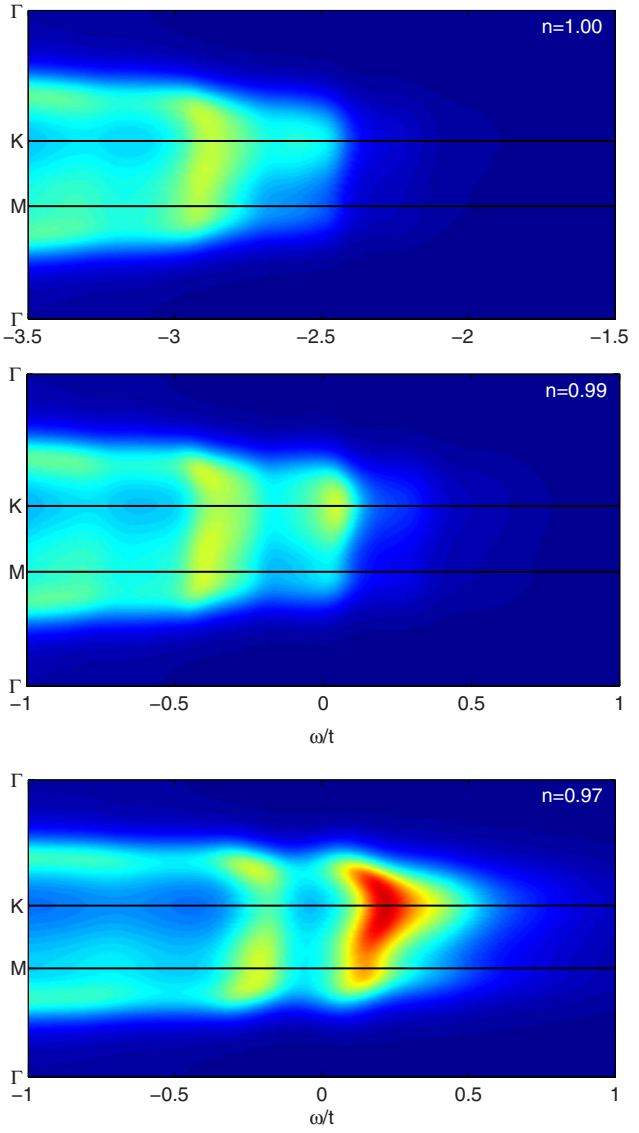

FIG. 20. (Color online) Comparison of the spectral function at half filling (top), 1% (middle) and 3% (bottom) hole doping, for the rhombic cluster at $U=12t$ and $T=0.1t$.

there is always a band that crosses the Fermi level even though the quasiparticle weight decreases closer to half filling. Consequently, using the diplike feature in the density of states as the criterion for the existence of a pseudogap, we conclude that no pseudogap exists for the Hubbard model on a triangular lattice for either electron or hole doping.

However, this analysis is incomplete. Let us approach the pseudogap problem from a different perspective. In the undoped cuprates, the quasiparticle dispersion below the Mott gap is characterized by four maxima at the $(\pm\pi/2, \pm\pi/2)$ points in the Brillouin zone, as revealed by ARPES measurements on $Ca_2CuO_2Cl_2$.[28] This feature is also present in the half-filled Hubbard model on a square lattice.[17] For a weakly (hole) doped system, if one adopts the naive picture of a rigid band shift, one would expect the chemical potential to move to the top of the lower Hubbard band and intersect it somewhere in the vicinity of the four minima. The resulting Fermi surface would consist of four small hole pockets in the

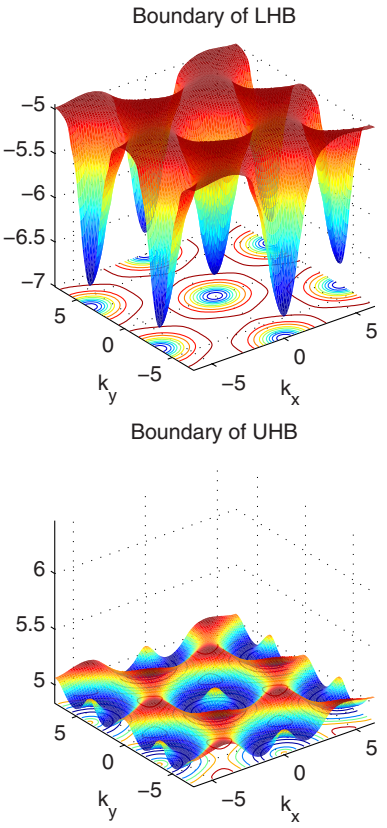

FIG. 21. (Color online) The boundary of the lower (top panel) and upper Hubbard bands (bottom panel) for $U=12t$ and $T=0.1t$.

vicinity of the $(\pm\pi/2, \pm\pi/2)$ points, while the rest of the large Fermi surface observed in optimally doped and overdoped cuprates (or at large doping values in the calculations for the Hubbard model) would be completely obliterated. That is, the low-energy excitations are gaped everywhere in the Brillouin zone, except on the boundary of the small Fermi pockets. This picture seems to be consistent with ARPES measurements on underdoped cuprates,[29] as well as the infrared Hall effect[30,31] and quantum oscillation measurements.[32] Nonetheless, strong-coupling calculations show that the naive rigid band picture is, in fact, incorrect and that strong correlations play a crucial role in pseudogap physics.

One of the essential aspects of strong correlations is spectral weight transfer. To illustrate its role, let us approach the pseudogap problem for Hubbard model on a triangular lattice starting from the Mott insulating phase. Note that, in contrast to the square-lattice model, in this case particle-hole symmetry is always absent and the antiferromagnetic interactions are frustrated. In Fig. 21 we show the top of the lower Hubbard band (top panel) and the bottom of the upper Hubbard band (bottom panel) for a half-filled system with $U=12t$. The two bands are separated by a Mott gap of about $5t$, and the chemical potential sits in the middle of the gap. The two surfaces are defined by the smallest frequencies at which the spectral function exceeds a certain small threshold δA. Variations in δA produce only small shifts of the two surfaces, but their shapes remain essentially the same. First, let us focus on the upper Hubbard band. As shown in Fig. 21, it is characterized by a set of minima along a large closed curve around the Γ point, not far from the Fermi surface corresponding to that of the noninteracting half-filled system. A small electron doping would move the chemical potential near this set of minima of the upper Hubbard band. In the rigid band picture, one ends up with two almost circular Fermi surfaces that define a narrow electron ring. However, our strong-coupling calculation leads to a different picture. Shown in Fig. 22 is the spectral function along the $\Gamma \rightarrow K \rightarrow M \rightarrow \Gamma$ path in the Brillouin zone and a small frequency window about the chemical potential for two small doping values. For comparison, we also show the bottom of the upper Hubbard band for the insulator (upper panel) within a similar frequency window. Note that for the insulator the bottom of the band corresponds to some middle points between Γ and K and between M and Γ. In the vicinity of the Γ point, there is no spectral weight within our frequency window (see also Fig. 21). However, once we dope the system, some spectral weight is transferred from high to low

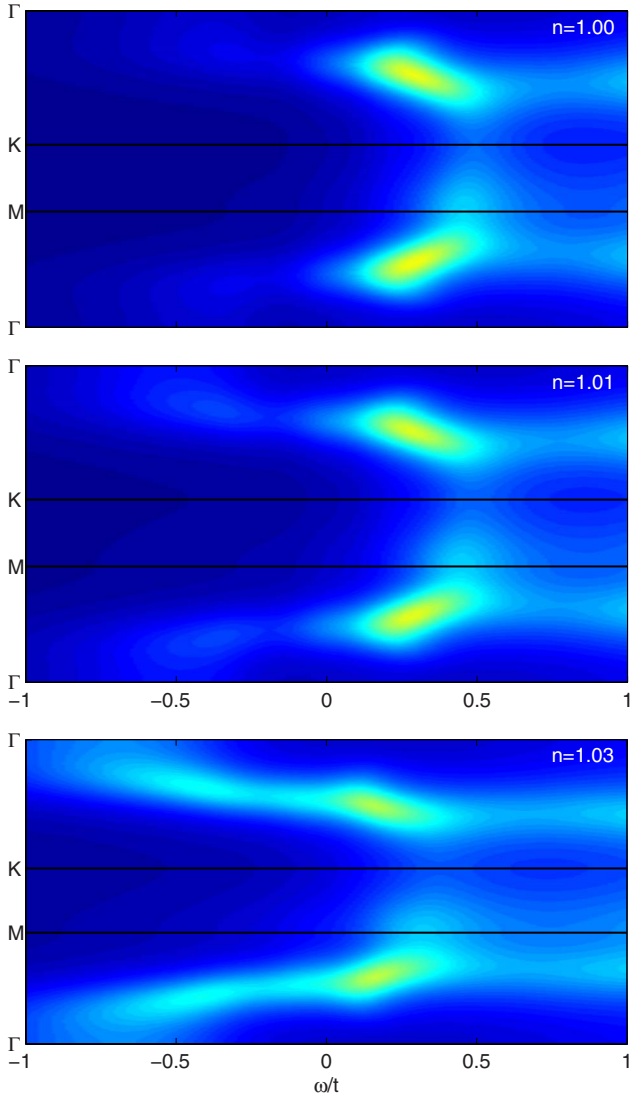

FIG. 22. (Color online) Comparison of the spectral function for half filling (top), 1% (middle) and 3% (bottom) electron doping, for the rhombic cluster at $U=12t$ and $T=0.1t$.

energies so that a low-energy band clearly forms in the vicinity of Γ just below the chemical potential. As a result, the strongly correlated narrow band that controls the low-energy physics disperses across the chemical potential generating a large Fermi surface consistent with the Luttinger theorem. A crucial difference from the square-lattice case is that the anisotropy along this large Fermi surface (or along the line defining the minima of the upper Hubbard band for the insulator) is very weak. By contrast, for the square lattice there is a qualitative difference between the $(\pi/2,\pi/2)$ and the $(0,\pi)$ regions of the Brillouin zone as illustrated, for example, by the existence of minima near the nodal points. This lack of anisotropy leads to the sudden appearance of a large Fermi surface upon doping and thus to the absence of a pseudogap.[33,34]

The situation appears somehow different in the case of the lower Hubbard band. As shown in Fig. 21, the top of the lower Hubbard band is extremely flat and extends over a significant portion of momentum space, all around the boundary of the Brillouin zone. Very weak maxima can be identified near the K points. In this case, the rigid band picture would suggest that a weakly hole-doped system is characterized by low-energy excitations that extend over a large portion of the Brillouin zone and that small Fermi pockets would possibly form near the K points and extend rapidly with doping. Again, in the vicinity of Γ there is no spectral weight at low energy. However, in contrast to the upper Hubbard band, this lack of low-energy excitations at small momenta persists upon doping. Shown in Fig. 20 is the low-energy spectral function along the same $\Gamma \rightarrow K \rightarrow M \rightarrow \Gamma$ path for the insulator (upper panel) and two values of doping. The relevant spectral weight transfer contributes this time to the reshaping of the low-energy narrow band that exists at momenta far from the Γ points. At increased doping values, this band becomes more dispersive and generates a large Fermi surface consistent with the noninteracting Fermi surface of a system with the same filling factor. Nonetheless, at very small doping values, several questions remain. First, it seems that the chemical potential crosses the narrow band in an extended area of the Brillouin zone rather than along a well-defined Fermi line. This stands in sharp contradiction with Fermi-liquid theory. However, one has to take into account that our results are obtained at a finite temperature of the order of $0.1t$, and thus the energy resolution is severely limited. To establish exactly the position of the Fermi surface at low dopings it would require a much better energy resolution and, consequently a much lower temperature, would be necessary. The second question concerns the existence of a pseudogap. One typically understands the pseudogap as a reduction in the number of low-energy modes below a certain energy scale. Here we propose a slightly different view. We define the pseudogap phase as a physical state occurring close to a Mott insulating state and characterized by the existence of small Fermi pockets with an area proportional to the doping level $x=1-n$. By contrast, a normal Fermi liquid is characterized by a large Fermi surface with an area that is related, via the Luttinger theorem, to the filling n. Consequently, one should view a system in the pseudogap phase as a doped Mott insulator. At the same time, the system represents a renormalized Fermi liquid characterized by a reconstructed Fermi surface. From this perspective, the weakly hole-doped Hubbard model on a triangular lattice is in the pseudogap state. Within the energy and momentum resolution of the present method, the Fermi surface appears as a set of small pockets around the K points that expand rapidly upon doping. A normal Fermi liquid is established at a doping level of a few percent. We emphasize that a crucial condition for the realization of this pseudogap phase was the existence of the small anisotropy in the lowest-energy excitations of the Mott insulator. To study in detail the formation and the evolution of the hole pockets, calculations using larger clusters (i.e., having a better momentum resolution) and lower temperatures are necessary.

V. CONCLUSIONS

We have studied a strongly correlated electron system on a triangular lattice using an implementation of the CDMFT+NCA scheme. The key technical aspects of this implementation are presented in detail. Numerical results are obtained for two types of clusters containing three and four sites, respectively. We stress that the cluster size analysis is a required step in any cluster DMFT-type calculation and argue that the relative invariance of the result against increasing the cluster size is the ultimate consistency criterion. The fundamental issue concerns the short-range vs long-range character of the electron correlations and the nature of the quantity that properly describes them. We find that the self-energy is not a short-range quantity in the vicinity of half filling and therefore cannot be captured using the cluster components. However, within our momentum and energy resolution, we find that the cumulant satisfies the locality requirements and can be used for reconstructing the lattice quantities. In this context, a very high priority for future cluster DMFT studies should be to establish the relevant range for the self-energy and the cumulant in various parameter regimes. Larger cluster calculations are required to clarify this point. Nonetheless, the task is of pivotal importance because if in a certain regime both the self-energy and the cumulant are long-ranged quantities the presently available real-space and momentum-space cluster DMFT schemes are not applicable.

At low doping values, we find that the Hubbard model on a triangular lattice is strongly correlated with low-energy physics controlled by a quasidispersionless band. As a result of correlations, the band is very narrow and its spectral weight can be transferred over large energy scales. A band with such features cannot be described by any weakly coupled approach. We also find that a metal-insulator transition occurs at a critical value of the on-site interaction $U_c \approx 5.6 \pm 0.15t$, which depends very weakly on the size of the cluster. This value is much lower than the critical interaction determined by $U_c \approx 10.5t$ in CDMFT calculations using exact diagonalization as the impurity solver,[10] but it is closer to $U_c \approx 6.9t$, which is the critical interaction obtained by continuous-time Monte Carlo.[11] Finally, we discussed the pseudogap problem in the context of the Hubbard model on a triangular lattice. In contrast to the square-lattice case, we find no evidence for a dip in the density of states positioned at the chemical potential. However, a momentum-resolved

analysis shows that the locus of the low-energy excitations of the weakly hole-doped system is qualitatively different from that of a noninteracting system. Therefore, we propose a framework for discussing the pseudogap phenomenon, which in essence involves a momentum-dependent characterization of the low-energy physics rather than a momentum-integrated one. We define a pseudogap state as a state characterized by low-energy excitations occurring only in a relatively small region in momentum space, qualitatively different from the location of the low-energy quasiparticles of the noninteracting system, and having an area that shrinks to zero when approaching the Mott insulator. Consequently, the system in the pseudogap state is characterized by a reconstructed Fermi surface consisting of small pockets. We find that the conditions necessary for the appearance of these pockets is a strongly momentum-dependent self-energy which produces quasiparticles with anisotropic properties along the Fermi surface. Therefore, the pseudogap is intrinsically linked to Mott physics as emphasized recently, which is the source of the long-range self-energy. Within the resolution of the present calculation, we find that the momentum dependence of the self-energy is much weaker for the triangular lattice, as compared to the square lattice, leading to a pseudogap only in the very weak hole-doped regime.

ACKNOWLEDGMENT

This work was supported in part by NSF under Contract No. DMR-0605769.

[1] D. J. Singh, Phys. Rev. B **61**, 13397 (2000).
[2] M. L. Foo, Y. Wang, S. Watauchi, H. W. Zandbergen, T. He, R. J. Cava, and N. P. Ong, Phys. Rev. Lett. **92**, 247001 (2004).
[3] M. Z. Hasan *et al.*, Phys. Rev. Lett. **92**, 246402 (2004).
[4] K.-W. Lee, J. Kuneš, P. Novak, and W. E. Pickett, Phys. Rev. Lett. **94**, 026403 (2005).
[5] D. Qian *et al.*, Phys. Rev. Lett. **96**, 216405 (2006).
[6] H.-B. Yang *et al.*, Phys. Rev. Lett. **95**, 146401 (2005).
[7] D. Qian *et al.*, Phys. Rev. Lett. **96**, 046407 (2006).
[8] H. Ishida, M. D. Johannes, and A. Liebsch, Phys. Rev. Lett. **94**, 196401 (2005).
[9] C. A. Marianetti, K. Haule, and O. Parcollet, Phys. Rev. Lett. **99**, 246404 (2007).
[10] B. Kyung, Phys. Rev. B **75**, 033102 (2007).
[11] H. Lee, G. Li, and H. Monien, arXiv:0807.1683 (unpublished).
[12] A. Georges, G. Kotliar, W. Krauth, and M. J. Rozenberg, Rev. Mod. Phys. **68**, 13 (1996).
[13] G. Kotliar, S. Y. Savrasov, G. Pálsson, and G. Biroli, Phys. Rev. Lett. **87**, 186401 (2001).
[14] P. Coleman, Phys. Rev. B **29**, 3035 (1984).
[15] G. Kotliar, S. Y. Savrasov, K. Haule, V. S. Oudovenko, O. Parcollet, and C. A. Marianetti, Rev. Mod. Phys. **78**, 865 (2006).
[16] T. D. Stanescu, M. Civelli, K. Haule, and G. Kotliar, Ann. Phys. **321**, 1682 (2006).
[17] T. D. Stanescu and G. Kotliar, Phys. Rev. B **74**, 125110 (2006).
[18] T. D. Stanescu, P. Phillips, and T.-P. Choy, Phys. Rev. B **75**, 104503 (2007).
[19] D. Qian, L. Wray, D. Hsieh, L. Viciu, R. J. Cava, J. L. Luo, D. Wu, N. L. Wang, and M. Z. Hasan, Phys. Rev. Lett. **97**, 186405 (2006).
[20] A. Rusydi *et al.*, Phys. Rev. B **78**, 125110 (2008).
[21] Y. Z. Zhang and M. Imada, Phys. Rev. B **76**, 045108 (2007).
[22] B. Kyung and A.-M. S. Tremblay, Phys. Rev. Lett. **97**, 046402 (2006).
[23] T. Maier, M. Jarrell, T. Pruschke, and M. H. Hettler, Rev. Mod. Phys. **77**, 1027 (2005).
[24] D. Wu, J. L. Luo, and N. L. Wang, Phys. Rev. B **73**, 014523 (2006).
[25] T. Shimojima *et al.*, Phys. Rev. B **71**, 020505 (2005).
[26] Y. Imai and N. Kawakami, Phys. Rev. B **65**, 233103 (2002).
[27] T. Ohashi, T. Momoi, H. Tsunetsugu, and N. Kawakami, Phys. Rev. Lett. **100**, 076402 (2008).
[28] A. Damascelli, Z. Hussain, and Z.-X. Shen, Rev. Mod. Phys. **75**, 473 (2003).
[29] K. M. Shen *et al.*, Science **307**, 901 (2005).
[30] L. B. Rigal, D. C. Schmadel, H. D. Drew, B. Maiorov, E. Osquiguil, J. S. Preston, R. Hughes, and G. D. Gu, Phys. Rev. Lett. **93**, 137002 (2004).
[31] A. Zimmers *et al.*, Phys. Rev. B **76**, 064515 (2007).
[32] N. Doiron-Leyraud, C. Proust, D. LeBoeuf, J. Levallois, J.-B. Bonnemaison, R. Liang, D. A. Bonn, W. N. Hardy, and L. Taillefer, Nature (London) **447**, 565 (2007).
[33] T.-P. Choy, R. G. Leigh, and P. Phillips, Phys. Rev. B **77**, 104524 (2008).
[34] P. Phillips, T.-P. Choy, and R. G. Leigh, arXiv:0802.3405 (unpublished).
[35] M. Hamermesh, *Group Theory and Its Application to Physical Problems* (Dover, New York, 1989).